Operando SWAXS for batteries

JPhys Energy

TUTORIAL • OPEN ACCESS

Operando SWAXS for batteries

To cite this article: X S Brems *et al* 2026 *J. Phys. Energy* **8** 023001

Journal of Physics: Energy

Check for updates

OPEN ACCESS

RECEIVED
18 January 2026

REVISED
23 March 2026

ACCEPTED FOR PUBLICATION
6 April 2026

PUBLISHED
28 April 2026

TUTORIAL

Operando SWAXS for batteries

X S Brems[1,3], M Olsson[2,3], A Matic[2,*] and S Lyonnard[1,*]

[1] University Grenoble Alpes, CEA, CNRS, Grenoble INP, IRIG, SyMMES, 38000 Grenoble, France
[2] Department of Physics and Astronomy, Chalmers University of Technology, Göteborg, Sweden
[3] Xaver S. Brems and Martina Olsson contributed equally.
[*] Authors to whom any correspondence should be addressed.

E-mail: matic@chalmers.se and sandrine.lyonnard@cea.fr

Keywords: SWAXS, operando, batteries, hard carbon, Si/graphite

Abstract

Advanced characterisation tools are needed to visualise and analyse the structural changes occurring in battery materials during cycling. Linking the electrochemical performance of the device to materials evolution is challenging as it requires to access microscopic information inside the system while it is working. As battery components are often multi-phase and multi-scale, the holistic analysis relies on combining or coupling techniques capable to reveal parameters of interest, such as local chemical properties, electronic structures, lattice parameters, morphology or chemomechanics. In this context, small angle and wide-angle x-ray scattering (SWAXS) techniques are complementary as they enable accessing the crystalline and amorphous/nanostructured phases. They are particularly suitable for probing composite or hierarchical materials at relevant length scales, including in real-time *operando* mode. In this tutorial article, we describe the principle of SWAXS, its applicability to battery research, and provide guidelines for conceiving, realizing and analysing SWAXS experiments. Beyond established set-ups where the averaged battery cell is probed in transmission or grazing incidence geometry, novel modalities using scanning and tomographic options are now available at 4th generation synchrotrons. These open new horizons to spatially-resolve reaction dynamics and associated (nano)structural heterogeneities, which is believed to be critical for in-depth mechanistic understanding and development of advanced materials. Here we illustrate the experimental approaches and workflows with two examples: silicon-graphite composites and hard carbons, both used as negative electrodes for Li-ion and Na-ion batteries, respectively. Archetypal data acquisition, reduction, processing and analysis methods are introduced, highlighting their advantages and pitfalls, while reporting a summary of key results and discoveries reported so far on the chosen examples. Finally, the future challenges for advanced SWAXS studies are discussed, encompassing novel beamtime access modes, data analysis strategies and development of AI-semi-automatised pipelines for high-throughput data correlations.

Glossary

SAXS	Small angle x-ray scattering, a technique to study structural changes on 1 – 100 nm length scales
WAXS	Wide angle x-ray scattering, a technique to study structural changes on Å length scales
GI-SWAXS	Small- and wide-angle x-ray scattering applied in a grazing incidence geometry to study surfaces and interfaces
μSWAXS	Small- and wide-angle x-ray scattering performed with a focused beam to spatially resolve on μm length scales scattering features
CT	Computed tomography which generates 3D images based on for instance absorption or scattering contrast

operando experiment	an investigation of a material or component directly in a working device at relevant conditions

1. Introduction

A challenge for battery materials and device research is the multiple length scales governing the electrochemical processes. Changes in crystalline materials during battery charge and discharge are usually followed by x-ray diffraction techniques (XRD), as (de)inserted ions induce phase transformations, solid solution behaviours, or distortions/strain of the crystalline lattice. However, a range of amorphous, nanoporous or nanostructured materials are also used as active materials or electrolytes for Li-ion, Na-ion and other battery technologies. In these cases, XRD provides limited information on their macro- and nanoscale structural evolution, whereas Small Angle x-ray Scattering is a powerful technique for determining the sizes, shapes, interactions, and distributions of nano-objects or nanophase-segregated domains [1, 2]. Indeed, it has been used either in *ex situ* or in *operando* mode to visualise and quantify nanoscale structural and compositional changes in different types of materials, from silicon-graphite anodes [3] and carbonaceous materials [4–6] to layered oxide cathodes [7], phosphate cathodes [8] or nanostructured liquids [9], polymer electrolytes [10] or sulphur systems [11]. Moreover, coupling SAXS to WAXS (so-called SWAXS approach) [3, 12, 13] is appealing to simultaneously cover multiple length scales and probe complex multicomponent materials. By providing structural and morphological information over multiple length scales of both ordered and disordered materials, it is highly complementary to *e.g.* XRD which can reveal the fine details of the atomic structure, and to spectroscopic methods such as x-ray absorption spectroscopy or x-ray photo emission spectroscopy, which rather provide information on the chemical state of the material.

Fourth-generation synchrotron sources based on diffraction-limited storage rings such as ESRF-EBS [14] and MAX IV [15] provide orders-of-magnitude higher brilliance and coherence, enabling *operando* SWAXS experiments on batteries with unprecedented temporal and spatial resolution. This enables the study of extremely fast phenomena, such as thermal runaway, as well as the use of scanning or tomographic methods. The latter open the route towards SWAXS imaging, which allows to reveal the 2D or 3D distribution of atomic and nanoscale features and their changes during battery operation. This is crucial for detecting reaction and degradation heterogeneities in electrodes within a working battery cell. SWAXS imaging has been demonstrated from model cells [16, 17] to follow detailed reaction mechanisms to commercial cell level [18]. SWAXS imaging, especially when applied in *operando* experiments, generates large datasets and requires the development of detailed workflows for data reduction and analysis.

In this tutorial, we provide a guide for experimental design and workflows for SWAXS experiments on battery materials and devices. We illustrate this through two state-of-the art examples, namely silicon-graphite composite electrodes for Li-ion and hard carbon electrodes for Na-ion batteries. We provide an overview of considerations for experimental design, including cell types, measurement modalities, and approaches to data reduction, processing, and analysis. We emphasise the possibilities for *operando* experiments, where we can follow processes within working battery cells in real time.

2. Experiment

A typical SWAXS experiment is schematically shown in figure 1(a). The x-ray beam impinges on the battery comprising the electrode stack (schematically shown in the inset) and scattered x-rays are collected using detectors located close or far from the sample for WAXS or SAXS, respectively, enabling to access scattering angles in the ranges 5°–30° and <5°, respectively. During an *operando* experiment, time-resolved 2D patterns are collected and radially averaged (in case of isotropic scattering, *i.e.* no directional dependence) to obtain the real-time 1D scattering curves in a q-range that typically spans from 10^{-3} to few Å^{-1} (figure 2) with q being the momentum transfer given by

$$q = \frac{4\pi}{\lambda}\sin\left(\theta\right) \tag{1}$$

where λ is the wavelength of the x-rays and 2θ is the scattering angle between the incoming and scattered x-rays.

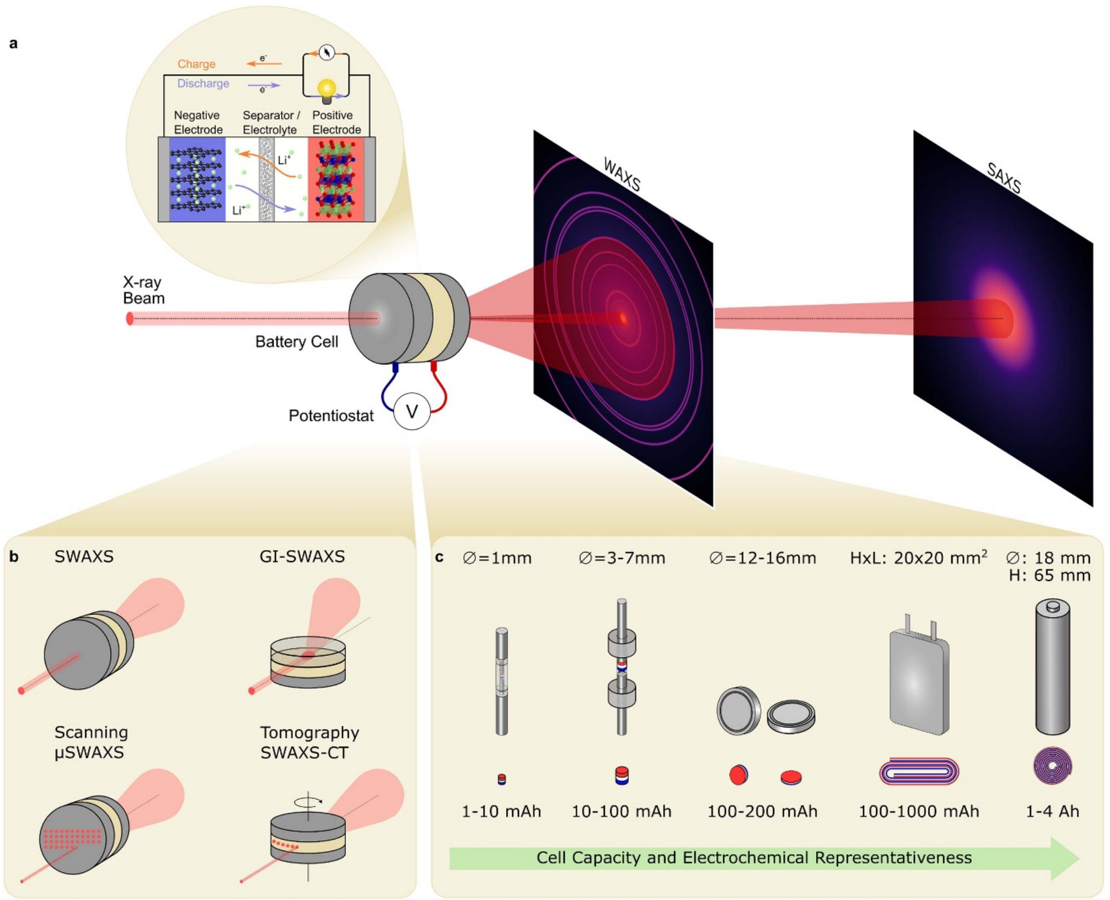

Figure 1. SWAXS set-up and experimental modalities. (a) An x-ray beam (energy in the range 1–100 keV; size 1–100 μm) is sent on the battery comprising the electrode stack (schematically shown in the inset). Scattered x-rays are collected on a 2D-detector which can be moved close (WAXS) or far (SAXS) from the sample. (b) Different measurement modalities depending on beam characteristics and measurement conditions: full field transmission geometry, grazing incidence (GI) geometry, scanning with a microbeam, or tomographic mode (SWAXS computed tomography). (c) Batteries with variable electrode stack orientations can be custom-made miniature cells, lab-scale formats such as coin/pouch cells, or real commercial formats, such as the cylindrical 18 650 cell, depending on the beamline capabilities and scientific interests.

The SWAXS scattering curve reflects all structures within the material at the probed length scales. Features appearing at low-q are related to larger structures while features at high-q reflect smaller structures. Following equation (1), the accessible q-values are determined by the wavelength and the accessible scattering angles. The magnitude of the wavelength is usually fixed for an experiment by the used x-ray source, with typical values ranging from 0.01–0.2 nm. Therefore, the accessible q-values are directly governed by the accessible scattering angles for a given wavelength and are a purely geometrical function of the experimental setup. The smallest accessible q-values (largest accessible real space length scale) depend on the maximum distance from the sample where the detector can be located, and the minimum size of/the minimum solid angle covered by the beamstop. The maximum q-value (smallest accessible length in real space) at a given sample-detector distance and wavelength is fixed by the dimension of the detector. Moving the detector to different locations or using several detectors simultaneously (e.g. with the WAXS detector positioned off-centre in the case of isotropic scattering, or having a hole at the direct beam point of incidence, as in figure 1) is common for extending the SWAXS q-range. Data taken with different set-ups are merged, enabling accessing features in real space across an extended range of scales, with sizes or correlation distances from 0.1 to several hundreds of nanometres typically.

3. Design

The design of an *operando* SWAXS experiment emerges from the interplay between the research question, the experimental capabilities, and the specifics and/or constraints of the operando cell, all of which are inherently intertwined. The nature of the incoming beam determines the spot size on the sample, ranging from millimeter-sized beams at laboratory sources to highly coherent nanobeams from fourth-generation synchrotron sources, as well as the type of experiments that can be performed (figure 1(b)). Generally, samples can be probed either in transmission (full field SWAXS) [3, 19], where all components in the beam path contribute to the measured signal, or in reflection mode (grazing incidence, GI-SWAXS) [8], which is suited to probe processes at interfaces or surfaces. The use of high brilliance microbeams from synchrotrons enables fast 2D scanning modes, useful to spatially resolve in-plane (*x*,*y*) [20, 21] or through-plane (*z*-profiling) [14] structural heterogeneities or phase distributions. This is of particular interest when aiming to capture the impact of cell design, manufacturing or operation conditions on, for example, the reaction mechanisms in battery electrodes, or to identify localised defects or specific damaged areas after long-term cycling or aging. Finally, 3D scattering imaging (SWAXS-CT) is also accessible by scanning and rotating the sample in the beam, performing tomographic measurements. Here, an image can be constructed based on a particular scattering feature (*e.g.* Bragg peaks in WAXS or nm features such as pores in SAXS). The resolution in SWAXS imaging is determined by the size of the microbeam, the spatial scanning step size and the angular steps (*i.e.* the number of projections) [16]. Each voxel in the 3D image contains the full SAXS and WAXS 2D patterns and the image can be reconstructed using tailored algorithms. SWAXS imaging experiments necessitate to compromise between space and time resolutions. *Operando* is achievable at low cycling rates (C-rates) on small cells, while high resolution on large formats must be performed *ex situ*.

The choice of beam specifics, experimental set-up and measurement modality depends both on the scientific question and characteristics of the battery cell to be investigated. A wide range of battery formats can be probed by SWAXS techniques [22], from miniature custom cells to large format commercial cells (figure 1(c)). The choice of one or the other option depends on the targeted research question and the acceptable trade-off between representative electrochemical performance, versus the desired level of precision and resolution, while also ensuring that the casing material and cell size are compatible with experimental setup and studied materials regarding absorption and expected scattering signals. Miniature custom Swagelok-type cells are developed to investigate structural evolution in vertically stacked electrode or electrolyte materials stacked, taking advantage of microbeams to scan the cell and resolve each component separately. This geometry is key to achieve depth-profiling, which is useful for instance to unravel concentration gradients as a function of C-rates or aging [23], or charge dynamics in graphite-silicon composite electrodes. These cells enable fast measurements using fly-scan modes and are also suitable for high resolution imaging. Standard lab-type batteries, *e.g.* coin cells, can be used, but require hard energy x-rays particularly if they are probed horizontally to allow penetration of the x-ray beam through the full electrode. Single-layer or multi-layer pouch cells can also be investigated [18, 19], with full high-resolution WAXS or SAXS 2D maps acquired within minutes at state-of-the-art synchrotron SWAXS instruments. At high energies above 70 keV, μSWAXS and SWAXS-CT can also be used to study small cylindrical cells [16] or even the larger 18 650 format cells, yielding unique views into the jelly-roll architecture and its changes during cycling or after long-term cycling. Additional constraints at cell level can also arise from the necessity to control stack pressure, as for solid-state batteries for instance [12], requiring to develop ad hoc designs. Further in-depth discussion on layout and design of *operando* cells can be found in [22, 24].

4. Data

Figures 2(a)–(d) describes a data analysis workflow, from pre-processing to interpretation, and a short checklist for data analysis following an experiment is found in box 1. First, the detector image is azimuthally integrated to obtain a 1D scattering curve (a) followed by transmission correction and background subtraction (b), producing the corrected curve for analysis. The analysis follows two main approaches: model-free analysis (c) and/or model-fitting (d). Model fitting provides details on structural parameters, but requires well-defined descriptors. In general, the scattering intensity can be described as $I(q) = N\Delta\rho^2 V^2 P(q)\,S(q)$, where N is the number density of scatterers, $\Delta\rho$ the electron density contrast, V the particle volume, $P(q)$ the form factor describing the particle shape of an individual particle, and $S(q)$ the structure factor describing interparticle correlations. This may be impractical for highly heterogeneous systems with overlapping scattering contributions and many different types of scatterers. A model-free approach is then a more robust/general (figure 2(c)) and can consider:

- **Porod and Guinier analysis:** SAXS curves often exhibit a decaying power law (Porod region) and shoulders (Guinier region). The positions of shoulders reflect structures with a characteristic size

Box.1. A practical checklist for data analysis

1. Inspect the 2D detector images to i) detect potential artefacts that should be masked (e.g. bad pixels or beam stop shadow) and ii) determine if there is anisotropy in the scattering, which may reveal structural orientation.
2. Convert the 2D detector images into 1D scattering curves by azimuthal integration. For anisotropic samples this may be done in segments to analyse different orientations.
3. Apply transmission corrections and correct for incident flux and exposure times.
4. Subtract the background contribution, ideally by measuring an empty cell or reference sample, to isolate the scattering contribution of the active material.
5. Initiate data interpretation by model-free analysis. Extract structural descriptors from features such as slopes, shoulders, peaks and oscillations in the curve.
6. Use the insight from the model-free analysis to determine if there is an analytical model that can be used for fitting the data and derive structural parameters.
7. (For imaging) Map the extracted structural descriptors or fitted parameters across the pixels to evaluate heterogeneities and spatial variations within the sample.

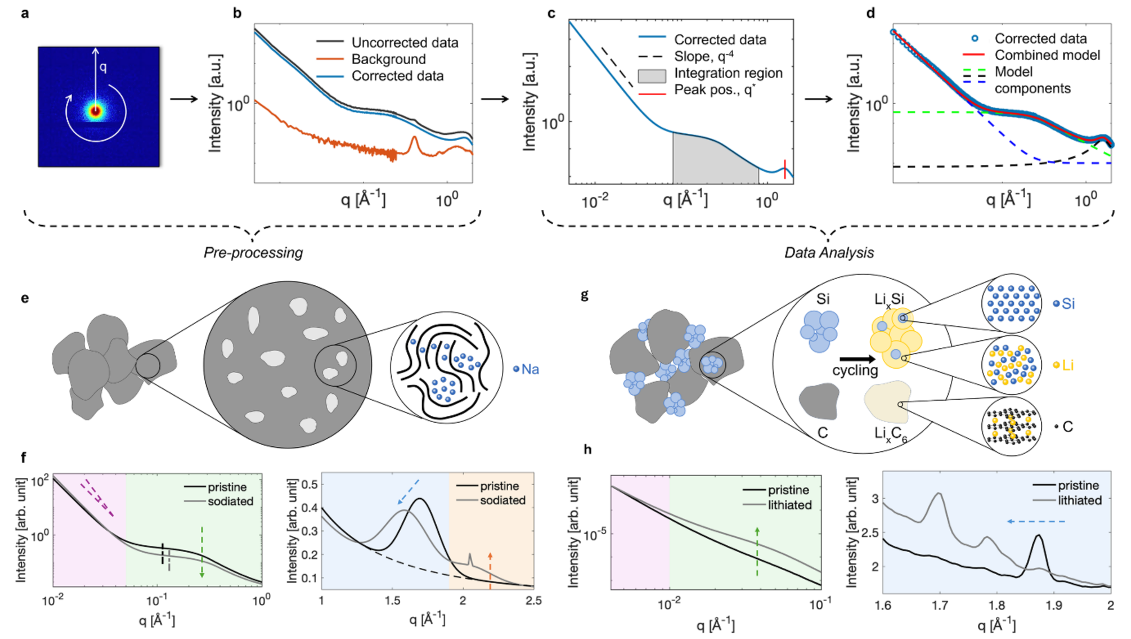

Figure 2. Workflow for data analysis and characteristic changes in structure and scattering exemplified for hard carbon and silicon-graphite composite electrodes. (a) In the pre-processing the detector images are first reduced into a scattering curve through azimuthal integration, (b) which is further corrected by transmission correction and background subtraction. The data analysis can then be performed through two main strategies: (c) model free analysis and/or (d) nonlinear fits to appropriate models to extract structural information. (e) Schematic of the hierarchical structure of sodiated hard carbon with microporous granular particles that consist of randomly arranged graphene layers where sodium can intercalate and fill the nanopores. (f) Characteristic scattering curves which display the typical changes observed from the pristine state (black) to the sodiated state (grey). (g) Schematic of the structure of lithiated composite silicon-graphite electrode material. (h) Characteristic scattering curves which display the typical changes observed from the pristine state (black) to the lithiated state (grey).

while the power law exponent provides information on surface morphology. The Guinier approximation; $I(q) = I(0)\exp\left(-q^2R_g^2/3\right)$ allows for extracting an objects radius of gyration , R_g, determining characteristic length scales in the sample. The power law exponent $I(q) \propto q^{-n}$ can reveal information on the morphology of scatterers, where $n \approx 4$ corresponds to scattering from sharp interfaces, $3 < n < 4$ indicates surface fractals and $1 < n < 3$ mass-fractals.

- **Integrated intensities:** Scattering intensity is related to the volume fraction and electron-density contrast of scatterers in a chosen q-region. For heterogenous materials, the integral over all q is a constant directly proportional to the mean-square average fluctuation in electron-density and phase composition. This is described as the scattering invariant; $Q = \int_0^\infty q^2 I(q)\,\mathrm{d}q$ and is independent of size and shape. Therefore, it can provide information about phase composition or changes in electron densities.

- **Peak analysis:** Position and width of a peak relate to lattice distances ($d^* = 2\pi/q^*$) and atomic order.
- **Oscillating features or shapes:** Local minima/bumps can reveal the existence of particular form factors.

We exemplify these analysis approaches with two model systems: sodiation of hard carbon and lithiation of silicon-graphite composite electrodes (figures 2(e)–(g)). The scattering curve from hard carbon shows a decaying slope (Porod regime) from particles followed by a shoulder related to nanopores in SAXS and a broad peak from stacked graphene layers in WAXS [4] (figure 2(f)). Filling of nanopores with sodium reduces the SAXS shoulder intensity as the electron-density contrast between nanopores and carbon matrix decreases [25–27] (green panel). Integrating the intensity in this q-region provides an estimate of the degree of pore filling, and pore size can be estimated by a Guinier fit of the shoulder [15]. During sodiation, intercalation induces interlayer expansion, leading to broadening and a shift of the WAXS peak to lower q (blue panel) [15, 22]. At higher q, densely packed sodium in the pores yields a broad structure peak, while formation of metallic sodium shows up as a sharp diffraction peak (orange panel).

The SAXS curve for a silicon-graphite composite electrode instead displays a featureless decaying intensity and a structure peak from graphite in WAXS (figure 2(h))[3]. Upon lithiation, a shoulder from silicon-rich Li_xSi domains appears in SAXS (green panel). The integrated intensity in this q-region reflects the degree of lithiation as it scales with the increased electron density difference of lithiated domains [3, 14, 16]. Moreover, the deviation from a power law provides a measure of swelling of silicon particles [14]. As silicon lithiation is an alloying process, a reduced silicon-domain structure-peak intensity is observed in WAXS along with partial amorphisation of crystalline silicon (blue panel), and a shift of the graphite peak to lower q due to interlayer expansion following intercalation.

5. Practical considerations

The experiment should be designed considering the structures of interest and the type of cell investigated. The sample-to-detector distance determines the covered q-range, which should match the length scales of interest, whereas the beam size on the sample decides the volume probed. In an imaging experiment the beam size determines the pixel size. A smaller beam generates higher resolution, but also increases measurement time when scanning the same field of view. Hence, a balance should be found between time and spatial resolution. Scanning SWAXS experiments can be performed on any sample shape, but sharp edges may introduce artefacts in tomographic reconstructions where the ideal shape is cylindrical for best reconstruction. One should also consider data handling when going to scanning or tomographic modalities, where an extended field of view combined with high spatial resolution results in very large data sets that can put constraints on or challenge data reduction and analysis.

Battery materials/electrodes are composed of several components, with different sizes/nature, or have a hierarchical distribution of objects. The resulting scattering profile can contain a combination of features, making Guinier analysis difficult due to overlapping contributions. Multiple Porod's regimes can be present, corresponding to individual pore/particle surfaces at high q, and grain or aggregate surfaces at low q. Polydispersity, polymorphism, and complex interactions among several components, also hinder quantitative form factor analysis. Instead, approaches using first or second derivatives can be attempted to highlight subtle changes in the intensity profiles due to volumetric or nanomorphological transformations. Another important consideration is the attenuation of the casing material and the casing contribution to the scattering signal. Quite often custom cells with x-ray transparent windows or low-attenuating materials, such as semicrystalline polymers, are used to ensure access to the inner components. However, while being highly transmissive to x-rays, semicrystalline polymers may produce strong SAXS and WAXS features that risk overlapping with the signals of interest.

A critical aspect for scattering and imaging experiments is beam damage, caused by interactions between the probed material and the x-ray beam, in the case of experiments at highly brilliant synchrotron sources (intense photon flux). This becomes particularly significant in *operando* experiments or high-resolution imaging which requires repeated exposures. Caution is needed to ensure that both the radiation dose and dose rate are within acceptable limits to not introduce artefacts or affect the electrochemistry. A good practice is to assess the radiation damage in a new material at the start of an experiment by increasing beam exposure and to calculate the accumulated dose that the sample is exposed to without introduction of artefacts. With this, a 'safe' operational dose interval can be determined. The 'safe' interval will depend on the materials investigated but as a reference a dose on the order of 1 MGy has been identified for standard graphite/NMC pouch cells [28]. Unnecessary exposure should be kept to a minimum by using filters to actively reduce photon flux as well as limit exposure times and number

Box.2. A practical checklist for beam damage mitigation

1. Determine a 'safe' dose range for the material system through repeated exposure tests.
2. Adjust experimental parameters to minimise exposure while preserving good enough signal and image resolution for the intended experiment.
3. Distribute beam exposure across the sample, when possible, *e.g.* by defocusing the beam or scanning in the sample.
4. If possible, define a separate area on the sample, that is scanned in scarce time intervals during the *operando* measurement at a reduced dose rate and serves as a control measurement.

of projections to match the resolution needed. In addition, especially for *operando* measurements, it is advisable to foresee a control area on the sample. The control area is probed at very scarce time intervals and much lower overall dose than the main scanning area and serves as a control measurement to detect any artefacts, which could be connected to beam damage [21]. A practical checklist for beam damage mitigation is included below in box 2.

6. Summary

SWAXS is an insightful tool to gather information on crystalline and nanostructured phases in battery materials and electrodes in one shot over multiple length scales, which is of great interest in a variety of battery chemistries, from Li-ion to Na-ion and beyond. The SWAXS modality is particularly useful to probe hierarchical, nanoporous, or mixed/composite materials and electrodes. Depending on the spatiotemporal resolution targeted, as well as the type of battery to be probed, specific x-ray beamlines and measurement modalities must be chosen. It is also important to point out that SWAXS can benefit from a combination with other tools, such as small angle neutron scattering (complementary as neutrons probe nuclei and are more sensitive to light elements), pair distribution function, or spectroscopic analysis to access local chemical or electronic properties. Moreover, additional detectors can be added *e.g.* to measure fluorescence [29], or SWAXS can be coupled and/or combined to/with sensing information (batteries equipped with optical fibres [22], gas detection [21], etc). Overall, AI-based analysis models are expected to be instrumental to take advantage of the full 2D/3D capabilities of SWAXS techniques in the future [30], and to develop correlative analysis of SWAXS datasets needed to fully reach the holistic understanding of battery behaviour.

Highly recommended/Further reading

Applications of SWAXS in fuel cell research: I. Martens *et al*, ACS energy Letters **6**, 2742 (2021).

Acknowledgments

The authors thank the European Battery Hub at ESRF (proposal MA6230). The work of SL is funded by French National Research Agency within the France2030 program (STORE-EX Labex Project ANR-10-LABX-76-01 and PEPR Batteries Project OPENSTORM ANR-22-PEBA-0005).

Data availability statement

No new data were created or analysed in this study.

Author contributions

X S Brems 0000-0002-0053-9116
Data curation (equal), Methodology (equal), Writing – original draft (equal), Writing – review & editing (equal)

M Olsson 0000-0003-2878-6239
Data curation (equal), Methodology (equal), Writing – original draft (equal), Writing – review & editing (equal)

A Matic 0000-0003-4414-9504
Conceptualization (equal), Resources (equal), Supervision (equal), Writing – original draft (equal), Writing – review & editing (equal)

S Lyonnard 0000-0003-2580-8439
Conceptualization (equal), Resources (equal), Supervision (equal), Writing – original draft (equal), Writing – review & editing (equal)

References

[1] Lee J, Park H, Kim H, Kim T, Jin M, Kim T and Kim J M 2023 Operando small-angle x-ray scattering for battery research *Bull. Korean Chem. Soc.* **44** 452
[2] Cheng W, Zhao M, Lai Y, Wang X, Liu H, Xiao P, Mo G, Liu B and Liu Y 2024 Recent advances in battery characterization using *in situ* XAFS, SAXS, XRD, and their combining techniques: from single scale to multiscale structure detection *Exploration* **4** 20230056
[3] Berhaut C, Dominguez D Z, Kumar P, Jouneau P-H, Porcher W, Aradilla D, Tardif S, Pouget S and Lyonnard S 2019 Multiscale multiphase lithiation and delithiation mechanisms in a composite electrode unraveled by simultaneous operando small-angle and wide-angle x-ray scattering *ACS Nano* **13** 11538
[4] Saurel D, Segalini J, Jauregui M, Pendashteh A, Daffos B, Simon P and Casas-Cabanas M 2021 A SAXS outlook on disordered carbonaceous materials for electrochemical energy storage *Energy Storage Mater.* **21** 162
[5] Härka E, Petzold A, Goerigk G, Risse S, Tallo I, Härmas R,Lust E and Ballauff M 2019 Carbide derived carbons investigated by small angle x-ray scattering: inner surface and porosity vs. graphitization *Carbon* **146** 84
[6] Jafta C, Petzold A, Risse S, Clemens D, Wallacher D, Goerigk G and Ballauff M 2017 Correlating pore size and shape to local disorder in microporous carbon: a combined small angle neutron and x-ray scattering study *Carbon* **123** 440
[7] Grenier A, Kamm G E, Li Y, Chung H, Meng Y S and Chapman K W 2021 Nanostructure transformation as a signature of oxygen redox in Li-rich 3d and 4d *J. Am. Chem. Soc.* **143** 5763
[8] Apfelbeck F A C *et al* 2024 Influence of the polymer binder composition on the charge transfer resistance, morphology, and crystallinity of $LiFePO_4$ electrodes revealed by electrochemical impedance spectroscopy and grazing incidence small- and wide-angle x-ray scattering *Small Sci.* **4** 240154
[9] Qian R E, Winans R E and Li T 2021 Insights into the nanostructure, solvation, and dynamics of liquid electrolytes through small-angle x-ray scattering *Adv. Energy Mater.* **11** 2002821
[10] Galluzzo M D, Loo W S, Schaible E, Zhu C and Balsara N P 2020 Dynamic structure and phase behavior of a block copolymer electrolyte under dc polarization *ACS Appl. Mater. Interfaces* **12** 57421s
[11] Prehal C, von Mentlen J-M, Drvarič Talian S, Vizintin A, Dominko R, Amenitsch H, Porcar L, Freunberger S A and Wood V 2022 On the nanoscale structural evolution of solid discharge products in lithium-sulfur batteries using operando scattering *Nat. Commun.* **13** 6326
[12] von Mentlen J-M 2025 Scanning SAXS/WAXS cell design for multiscale analysis of all-solid-state battery systems *Batteries Supercaps* **8** e202500428
[13] Povia M, Sottmann J, Portale G, Knudsen K D, Margadonna S and Sartori S 2018 Operando SAXS/WAXS on the a-P/C as the anode for Na-Ion batteries *J. Phys. Chem. C* **122** 5917
[14] Raimondi P *et al* 2023 The extremely brilliant source storage ring of the European sycnhrotron radiation facility *Commun. Phys.* **6** 82
[15] Tavares P F, Leeman S C, Sjöström M and Andersson Å 2014 The MAX IV storage ring project *J. Synchrotron Radiat.* **21** 862
[16] Berhaut C L, Mirolo M, Dominguez D Z, Martens I, Pouget S, Herlin-Boime N, Chandesris M, Tardif S, Drnec J and Lyonnard S 2023 Charge dynamics induced by lithiation heterogeneity in silicon-graphite composite anodes *Adv. Energy Mater.* **13** 2301874
[17] Olsson M, Klein A, Mozhzhukhina N, Xiong S, Appel C, Carlsen M, Nielsen L, Rensmo L, Liebi M and Matic A 2025 Resolving the sodiation process in hard carbon anodes with nanostructure specific X-ray imaging *Adv. Sci.* **11** e08635
[18] Lübke E *et al* 2024 The origins of critical deformations in cylindrical silicon based Li-ion batteries *Energy Environ. Sci.* **17** 5048
[19] Berhaut C L *et al* 2020 Prelithiation of silicon/graphite composite anodes: benefits and mechanisms for long-lasting Li-Ion batteries *Energy Storage Mater.* **29** 190
[20] Jacquet Q, Profatilova I, Baggetto L, Alrifai B, Addes E, Chassagne P, Blanc N, Tardif S, Daniel L and Lyonnard S 2024 Mapping reaction mechanism during overcharge of a LiNiO2/graphite–silicon lithium-ion battery: a correlative operando approach by simultaneous gas analysis and synchrotron scattering techniques *Adv. Energy Mater.* **15** 2404080
[21] Olgo A *et al* 2024 The local impact of sensors on a commercial Li-ion battery pouch cell graphite electrode lithiation mechanism *Nat. Commun.* **15** 10258
[22] Atkins D *et al* 2022 Accelerating battery characterization, using neutron and sycnhrotron technqiues: toward a multi-modal and multi-scale standardized experimental workflow *Adv. Energy Mater.* **12** 2102694
[23] Oney G *et al* 2025 Dead, slow and overworked graphite: operando x-ray microdiffraction mapping of aged electrodes *Adv. Energy Mater.* **14** e02032
[24] Bak S-M, Shadike Z, Lin R, Yu X and Yang X-Q 1018 In situ/operando synchrotron-based x-ray techniques for lithium-ion battery reserach *NPG Asia Mater.* **10** 563
[25] Morikawa Y, Nishimura S-I, Hashimoto R-I, Ohnuma M and Yamada A 2020 Mechanism of sodium storage in hard carbon: an x-ray scattering analysis *Adv. Energy Mater.* **10** 1903176
[26] Stevens D and Dahn J 2000 An in situ small-angle x-ray scattering study of sodium insertion into a nanoporous carbon anode material within an operating electrochemical cell *J. Electrochem. Soc.* **147** 4428
[27] Kitsu Iglesias L, Antonio E N, Martinez T D, Zhang L, Zhuo Z, Weigand S J, Guo J and Toney M F 2023 Revealing the sodium storage mechanisms in hard carbon pores *Adv. Energy Mater.* **13** 2302171

[28] Jousseaume T, Colin J-F, Chandesris M, Lyonnard S and Tardif S 2023 How beam damage can skew synchrotron operando studies of batteries *ACS Energy Lett.* **8** 3323

[29] Dawkins J I, Martens I, Danis A, Beaulieu I, Chhin D, Mirolo M, Drnec J, Schougaard S B and Mauzeroll J 2023 Mapping the total lithium inventory of Li-ion batteries *Joule* **7** 2783

[30] Monge N, Deschamps A and Amini M-R 2024 Automated selection of nanoparticle models for small-angle x-ray scattering data analysis using machine learning *Acta Crystallogr.* **80** 202